Electronic Supplementary Material (ESI) for Dalton Transactions.

# Solution and solid state structures and magnetism of a series of linear trinuclear compounds with a hexacoordinate $Ln^{III}$ and two terminal $Ni^{II}$ centers

*Peter Comba,[1,2]* Markus Enders,[1]* Michael Großhauser,[1] Markus Hiller,[1] Dennis Müller,[1,2] and Hubert Wadepohl[1]*

[1] Universität Heidelberg, Anorganisch-Chemisches Institut INF 270, D-69120 Heidelberg, Germany

[2] Interdisziplinäres Zentrum für Wissenschaftliches Rechnen, IWR, INF 270, D-69120 Heidelberg, Germany

# Electronic Supporting Information

Correspondence:

Fax: +49-6221-546617

E-mail: peter.comba@aci.uni-heidelberg.de

E-Mail: markus.enders@uni-heidelberg.de

# 1. X-ray Crystal Structure Determinations

Crystal data and details of the structure determinations are compiled in Tables S1a – S1c. Full shells of intensity data were collected at low temperature with a Bruker AXS Smart 1000 CCD diffractometer (Mo-$K_\alpha$ radiation, sealed X-ray tube, graphite monochromator) or an Agilent Technologies Supernova-E CCD diffractometer (Mo- or Cu-$K_\alpha$ radiation, microfocus X-ray tube, multilayer mirror optics). Data were corrected for air and detector absorption, Lorentz and polarization effects;[1-3] absorption by the crystal was treated numerically (Gaussian grid) or with a semiempirical multiscan method.[3-7] The structures were solved by the charge flip procedure[8, 9] and refined by full-matrix least squares methods based on $F^2$ against all unique reflections.[10-12] All non-hydrogen atoms were given anisotropic displacement parameters. Hydrogen atoms were input at calculated positions and refined with a riding model. The perchlorate anions were frequently found disordered. When possible, split atom models were used and/or appropriate geometry and adp restraints were applied. Due to severe disorder and/or fractional occupancy, electron density attributed to solvent of crystallization (methanol, water, dichloromethane and perhaps triethylamine) was removed from the structures with $L_n$ = Y, La, Ce, Nd, Er, Tm and Lu with the BYPASS procedure,[13, 14] as implemented in PLATON (SQUEEZE).[15, 16] Partial structure factors from the solvent masks were included in the refinement as separate contributions to $F_{obs}$.

CCDC 1458673 - 1458686 contains the supplementary crystallographic data for this paper. These data can be obtained free of charge from The Cambridge Crystallographic Data Centre via www.ccdc.cam.ac.uk/data_request/cif.

**Table S1a.** Details of the crystal structure determinations of $Ni^{II}_2Ln^{III}$ complexes (Ln = Y, La, Ce, Nd, Sm).

| | **Ln = Y (·*x* MeOH)** | **Ln = La (· solv)** | **Ln = Ce (· solv)** | **Ln = Nd (· solv)** | **Ln = Sm (· MeOH)** |
|---|---|---|---|---|---|
| formula | $C_{66}H_{84}ClN_6Ni_2O_{16}Y$ | $C_{66}H_{84}Cl_2LaN_6Ni_2O_{20}$ | $C_{66}H_{84}CeC_{l2}N_6Ni_2O_{20}$ | $C_{66}H_{84}C_{l2}N_6NdNi_2O_{20}$ | $C_{68}H_{94}ClN_6Ni_2O_{19}Sm$ |
| crystal system | monoclinic | orthorhombic | orthorhombic | orthorhombic | monoclinic |
| space group | *C* 2/*c* | *P nna* | *P nna* | *P nna* | *C* 2/*c* |
| *a* /Å | 20.088(10) | 12.90542(15) | 12.91505(16) | 12.94563(15) | 19.645(10) |
| *b* /Å | 21.319(11) | 25.5630(3) | 25.5924(3) | 25.5344(3) | 18.946(10) |
| *c* /Å | 17.532(9) | 22.9782(3) | 22.9435(3) | 22.9043(3) | 19.212(10) |
| $\beta$ /° | 106.603(11) | | | | 109.102(12) |
| *V* /Å$^3$ | 7195(6) | 7580.53(15) | 7583.44(16) | 7571.21(16) | 6757(6) |
| *Z* | 4 | 4 | 4 | 4 | 4 |
| $M_r$ | 1459.17 | 1608.62 | 1609.83 | 1613.95 | 1602.71 |
| $F_{000}$ | 3048 | 3316 | 3320 | 3328 | 3324 |
| $d_c$ /Mg·m$^{-3}$ | 1.347 | 1.409 | 1.410 | 1.416 | 1.576 |
| μ /mm$^{-1}$ | 1.421 | 1.186 | 1.222 | 1.309 | 1.527 |
| max., min. transmission factors | 0.6478, 0.5872 [a] | 0.903, 0.803 [b] | 0.899, 0.818 [b] | 0.910, 0.821 [b] | 0.8497, 0.7481 [a] |
| X-radiation, $\lambda$ /Å | Mo-*K*α, 0.71073 | Mo-*K*α, 0.71073 | Mo-*K*α, 0.71073 | Mo-*K*α, 0.71073 | Mo-*K*α, 0.71073 |
| data collect. temperat. /K | 100(1) | 120(1) | 120(1) | 120(1) | 100(1) |
| $\theta$ range /° | 1.9 to 30.6 | 3.3 to 29.0 | 3.3 to 29.0 | 3.4 to 29.0 | 2.1to 30.6 |
| index ranges *h*,*k*,*l* | -28 ... 28, -30 ... 30, -25 ... 25 | -17 ... 17, -34 ... 33, -31 ... 29 | -17 ... 17, -34 ... 34, -31 ... 30 | -17 ... 17, -34 ... 34, -29 ... 30 | -28 ... 28, -27 ... 27, -27 ... 27 |
| reflections measured | 88180 | 257031 | 196125 | 163640 | 81387 |
| unique [$R_{int}$] | 11002 [0.0411] | 9906 [0.0589] | 9830 [0.0534] | 9766 [0.0484] | 10382 [0.0555] |
| observed [$I \geq 2\sigma(I)$] | 9206 | 8466 | 9123 | 8982 | 8691 |
| data / restraints /parameters | 11002 / 51 / 444 | 9906 / 51 / 444 | 9830 / 51 / 444 | 9766 / 51 / 444 | 10382 / 24 / 468 |
| GooF on $F^2$ | 1.048 | 1.073 | 1.217 | 1.169 | 1.055 |

| | **Ln = Y (·*x* MeOH)** | **Ln = La (· solv)** | **Ln = Ce (· solv)** | **Ln = Nd (· solv)** | **Ln = Sm (· MeOH)** |
|---|---|---|---|---|---|
| *R* indices [$F>4\sigma(F)$] $R(F)$, $wR(F^2)$ | 0.0469, 0.1423 | 0.0614, 0.1722 | 0.0775, 0.1796 | 0.0671, 0.1655 | 0.0330, 0.0771 |
| *R* indices (all data) $R(F)$, $wR(F^2)$ | 0.0581, 0.1511 | 0.0718, 0.1788 | 0.0834, 0.1823 | 0.0729, 0.1683 | 0.0461, 0.0833 |
| largest residual peaks /e·$Å^{-3}$ | 3.125, -0.875 | 2.577, -1.949 | 1.932, -1.932 | 2.169, -1.932 | 1.405, -0.695 |
| instrument | Smart 1000 | Supernova E | Supernova E | Supernova E | Smart 1000 |

[a] empirical absorption correction; [b] numerical absorption correction.

**Table S1b.** Details of the crystal structure determinations of $\mathrm{Ni^{II}}_2\mathrm{Ln^{III}}$ complexes (Ln = Eu, Gd, Tb, Dy).

| | **Ln = Eu (· MeOH)** | **Ln = Gd** | **Ln = Tb (· MeOH)** | **Ln = Dy (· MeOH)** | **Ln = Dy** |
|---|---|---|---|---|---|
| formula | $C_{68}H_{94}ClEuN_6Ni_2O_{19}$ | $C_{66}H_{84}ClGdN_6Ni_2O_{16}$ | $C_{68}H_{94}ClN_6Ni_2O_{19}Tb$ | $C_{67}H_{88}ClDyN_6Ni_2O_{17}$ | $C_{66}H_{84}ClDyN_6Ni_2O_{16}$ |
| crystal system | monoclinic | monoclinic | monoclinic | monoclinic | monoclinic |
| space group | $C\ 2/c$ | $P\ 2_1/n$ | $C\ 2/c$ | $P\ 2_1/n$ | $P\ 2_1/n$ |
| $a$ /Å | 19.679(10) | 12.863(7) | 19.7091(2) | 14.600(6) | 12.89637(9) |
| $b$ /Å | 18.955(10) | 22.430(11) | 18.98270(18) | 25.289(10) | 22.41000(15) |
| $c$ /Å | 19.191(10) | 23.022(11) | 19.1549(2) | 18.680(8) | 23.03847(16) |
| $\beta$ /° | 109.106(11) | 93.909(15) | 109.0376(12) | 99.199(11) | 93.3859(6) |
| $V$ /Å$^3$ | 6765(6) | 6627(6) | 6774.48(13) | 6808(5) | 6646.67(8) |
| $Z$ | 4 | 4 | 4 | 4 | 4 |
| $M_r$ | 1604.32 | 1527.51 | 1611.28 | 1564.80 | 1532.76 |
| $F_{000}$ | 3328 | 3148 | 3336 | 3228 | 3156 |
| $d_c$ /Mg·m$^{-3}$ | 1.575 | 1.531 | 1.580 | 1.527 | 1.532 |
| $\mu$ /mm$^{-1}$ | 1.584 | 1.664 | 1.700 | 1.746 | 1.785 |
| max., min. transmission factors | 0.8498, 0.7500 [a] | 0.7464, 0.6663 [a] | 0.887, 0.793 [b] | 0.7464, 0.6992 [a] | 1.0000, 0.9214 [a] |
| X-radiation, $\lambda$ /Å | Mo-$K\alpha$, 0.71073 | Mo-$K\alpha$, 0.71073 | Mo-$K\alpha$, 0.71073 | Mo-$K\alpha$, 0.71073 | Mo-$K\alpha$, 0.71073 |
| data collect. temperat. /K | 100(1) | 100(1) | 120(1) | 100(1) | 120(1) |
| $\theta$ range /° | 2.1 to 32.5 | 1.8 to 32.5 | 3.3 to 29.0 | 2.1 to 32.5 | 3.2 to 32.8 |
| index ranges $h,k,l$ | -29 ... 29, -28 ... 27, -28 ... 27 | -19 ... 19, -33 ... 33, -33 ... 33 | -26 ... 26, -25 ... 25, -25 ... 25 | -21 ... 22, -37 ... 36, -28 ... 28 | -19 ... 19, -33 ... 34, -35 ... 34 |
| reflections measured | 85272 | 167930 | 94491 | 174087 | 222510 |
| unique [$R_{int}$] | 11667 [0.0478] | 22856 [0.0497] | 8626 [0.0409] | 23456 [0.0338] | 23387 [0.0537] |
| observed [$I \geq 2\sigma(I)$] | 9866 | 18546 | 8333 | 20699 | 20243 |
| data / restraints /parameters | 11667 / 24 / 468 | 22856 / 21 / 840 | 8626 / 24 / 468 | 23456 / 21 / 861 | 23387 / 21 / 840 |
| GooF on $F^2$ | 1.054 | 1.100 | 1.181 | 1.056 | 1.093 |
| $R$ indices [$F>4\sigma(F)$] $R(F)$, $wR(F^2)$ | 0.0298, 0.0632 | 0.0393, 0.0850 | 0.0308, 0.0661 | 0.0293, 0.0696 | 0.0335, 0.0737 |

| | **Ln = Eu (· MeOH)** | **Ln = Gd** | **Ln = Tb (· MeOH)** | **Ln = Dy (· MeOH)** | **Ln = Dy** |
|---|---|---|---|---|---|
| *R* indices (all data) $R(F)$, $wR(F^2)$ | 0.0429, 0.0683 | 0.0577, 0.0939 | 0.0330, 0.0668 | 0.0364, 0.0736 | 0.0431, 0.0771 |
| largest residual peaks /e·Å$^{-3}$ | 1.014, -0.609 | 2.835, -0.863 | 0.686, -0.781 | 1.705, -1.531 | 0.877, -0.724 |
| instrument | Smart 1000 | Smart 1000 | Supernova E | Smart 1000 | Smart 1000 |

[a] empirical absorption correction; [b] numerical absorption correction

**Table S1c.** Details of the crystal structure determinations of $Ni^{II}_2Ln^{III}$ complexes (Ln = Ho, Er, Tm, Lu).

| | **Ln = Ho** | **Ln = Er (·*x* MeOH)** | **Ln = Tm (· solv)** | **Ln = Lu (· solv)** |
|---|---|---|---|---|
| formula | $C_{66}H_{84}ClHoN_6Ni_2O_{16}$ | $C_{66}H_{84}ClErN_6Ni_2O_{16}$ | $C_{68}H_{88}Cl_5N_6Ni_2O_{16}Tm$ | $C_{66}H_{84}ClLuN_6Ni_2O_{16}$ |
| crystal system | monoclinic | monoclinic | monoclinic | monoclinic |
| space group | $P\,2_1/n$ | $C\,2/c$ | $P\,2_1/c$ | $P\,2_1/c$ |
| $a$ /Å | 12.862(8) | 20.090(9) | 20.3567(4) | 20.5007(7) |
| $b$ /Å | 22.398(14) | 21.331(9) | 23.5628(3) | 23.1939(5) |
| $c$ /Å | 23.026(13) | 17.493(7) | 18.0810(3) | 18.0326(5) |
| $\beta$ /° | 93.048(9) | 106.643(8) | 116.335(2) | 114.771(4) |
| $V$ /Å$^3$ | 6624(7) | 7183(5) | 7772.7(3) | 7785.4(4) |
| $Z$ | 4 | 4 | 4 | 4 |
| $M_r$ | 1535.19 | 1537.52 | 1709.04 | 1545.23 |
| $F_{000}$ | 3160 | 3164 | 3504 | 3176 |
| $d_c$ /Mg·m$^{-3}$ | 1.539 | 1.422 | 1.460 | 1.318 |
| μ /mm$^{-1}$ | 1.858 | 1.780 | 4.739 | 1.833 |
| max., min. transmission factors | 0.8136, 0.7257 [a] | 0.3012, 0.2570 [a] | 0.881, 0.603 [b] | 0.987, 0.913 [b] |
| X-radiation, $\lambda$ /Å | Mo-$K\alpha$, 0.71073 | Mo-$K\alpha$, 0.71073 | Cu-$K\alpha$, 1.54184 | Mo-$K\alpha$, 0.71073 |
| data collect. temperat. /K | 100(1) | 100(1) | 120(1) | 120(1) |
| $\theta$ range /° | 1.9 to 31.5 | 1.4 to 32.5 | 3.8 to 71.1 | 3.3 to 26.4 |
| index ranges $h,k,l$ | -18 ... 18, -32 ... 32, -33 ... 33 | -29 ... 30, -30 ... 32, -26 ... 26 | -24 ... 24, -28 ... 28, -22 ... 22 | -25 ... 25, -29 ... 28, -22 ... 22 |
| reflections measured | 165056 | 91595 | 210562 | 157031 |
| unique [$R_{int}$] | 21966 [0.0614] | 12409 [0.0392] | 14914 [0.0849] | 15932 [0.1540] |
| observed [$I \geq 2\sigma(I)$] | 17268 | 10847 | 12731 | 11968 |
| data / restraints /parameters | 21966 / 21 / 840 | 12409 / 51 / 444 | 14914 / 28 / 895 | 15932 / 0 / 841 |
| GooF on $F^2$ | 1.049 | 1.059 | 1.048 | 1.096 |
| $R$ indices [$F>4\sigma(F)$] $R(F)$, $wR(F^2)$ | 0.0357, 0.0679 | 0.0347, 0.1004 | 0.0552, 0.1449 | 0.0594, 0.1174 |

| | **Ln = Ho** | **Ln = Er (·*x* MeOH)** | **Ln = Tm (· solv)** | **Ln = Lu (· solv)** |
|---|---|---|---|---|
| *R* indices (all data) $R(F)$, $wR(F^2)$ | 0.0575, 0.0747 | 0.0432, 0.1068 | 0.0654, 0.1515 | 0.0865, 0.1253 |
| largest residual peaks /e·Å$^{-3}$ | 1.148, -0.774 | 3.329, -0.761 | 2.043, -2.051 | 0.926, -0.762 |
| instrument | Supernova E | Smart 1000 | Supernova E | Supernova E |

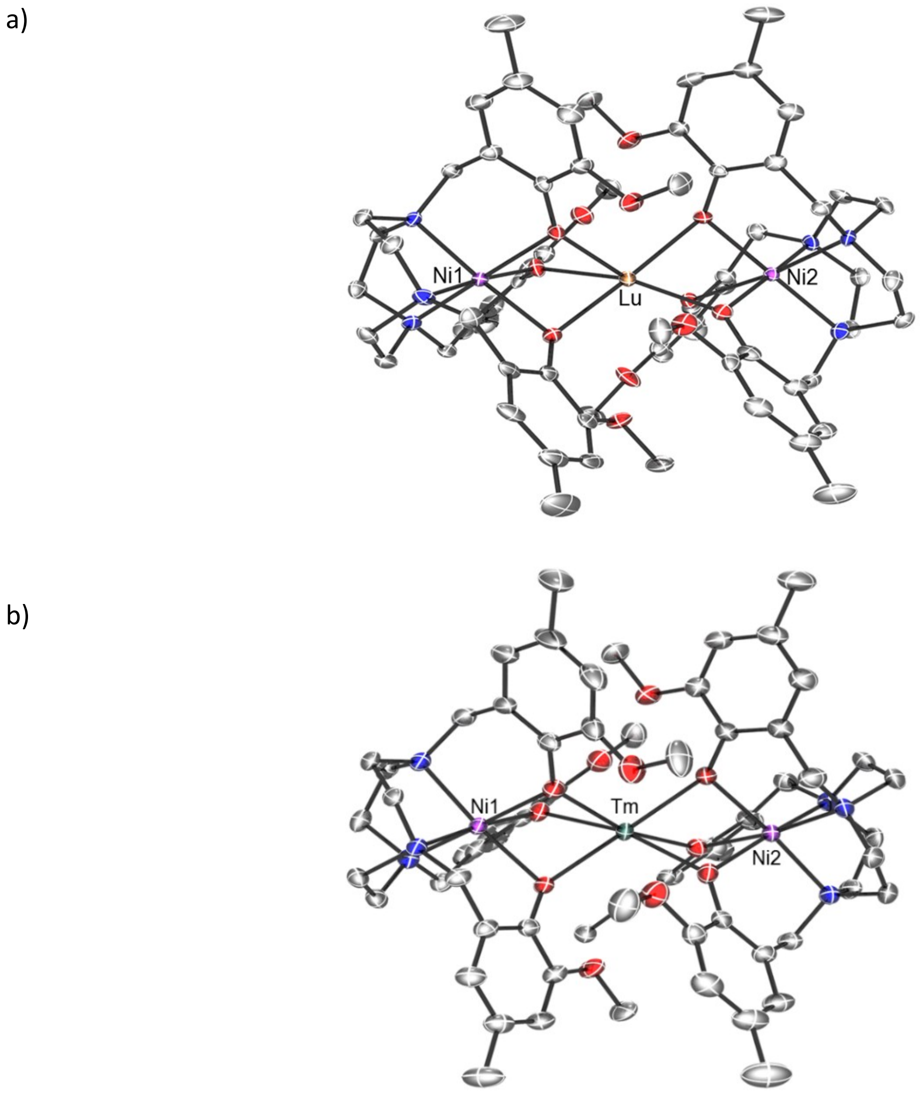

**Figure S1.** Structural plots of $Ni^{II}_2Ln^{III}$ (ORTEP plots with 50% probability level of the thermal ellipsoids, hydrogen atoms omitted): a) $[Y^{III}\{Ni^{II}(L)\}_2]ClO_4 \cdot 1.5\ H_2O$, b) $[La^{III}\{Ni^{II}(L)\}_2]ClO_4$, c) $[Ce^{III}\{Ni^{II}(L)\}_2]ClO_4$, d) $[Nd^{III}\{Ni^{II}(L)\}_2]ClO_4$, e) $[Sm^{III}\{Ni^{II}(L)\}_2OH_2]ClO_4$, f) $[Eu^{III}\{Ni^{II}(L)\}_2OH_2]ClO_4$, g) $[Gd^{III}\{Ni^{II}(L)\}_2]ClO_4 \cdot 2\ H_2O$, h) $[Tb^{III}\{Ni^{II}(L)\}_2OH_2]ClO_4 \cdot H_2O$, i) $[Dy^{III}\{Ni^{II}(L)\}_2]ClO_4$, j) $[Ho^{III}\{Ni^{II}(L)\}_2]ClO_4 \cdot 2\ H_2O$, k) $[Er^{III}\{Ni^{II}(L)\}_2]ClO_4$, l) $[Tm^{III}\{Ni^{II}(L)\}_2]ClO_4$, m) $[Lu^{III}\{Ni^{II}(L)\}_2]ClO_4$.

c)

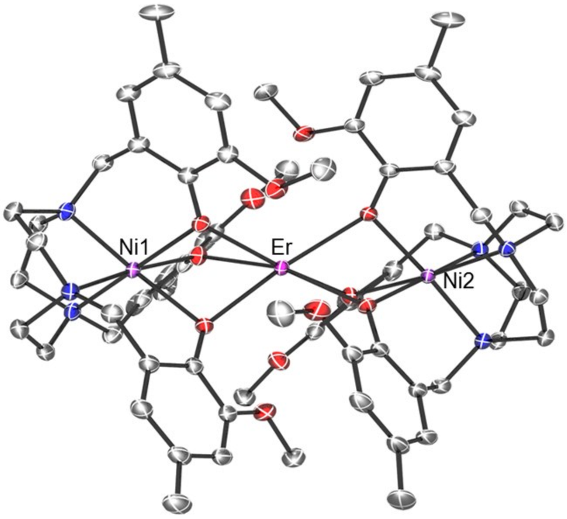

d)

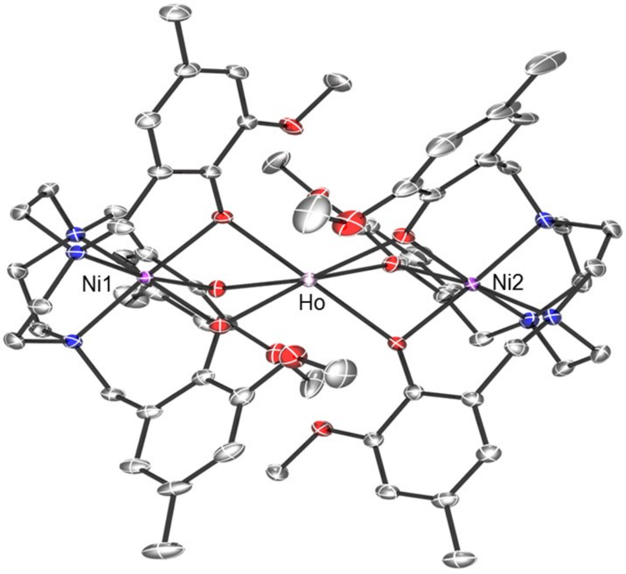

**Figure S1.** continued

e)

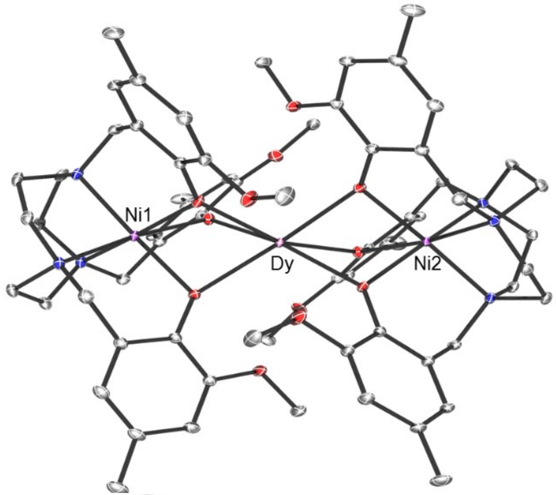

f)

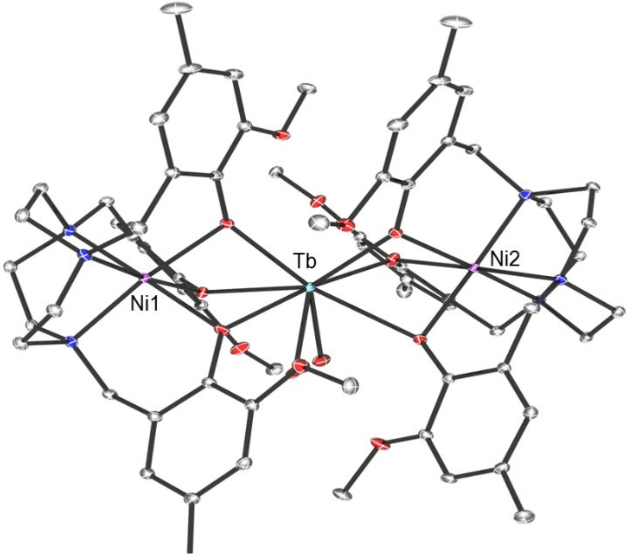

**Figure S1.** continued

g)

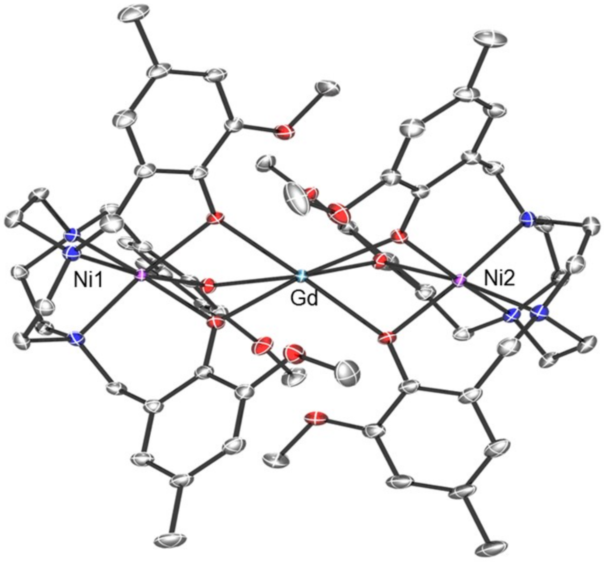

h)

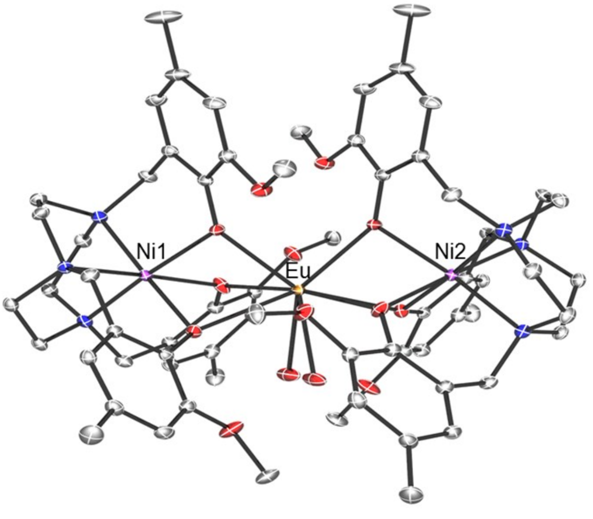

**Figure S1.** continued

i)

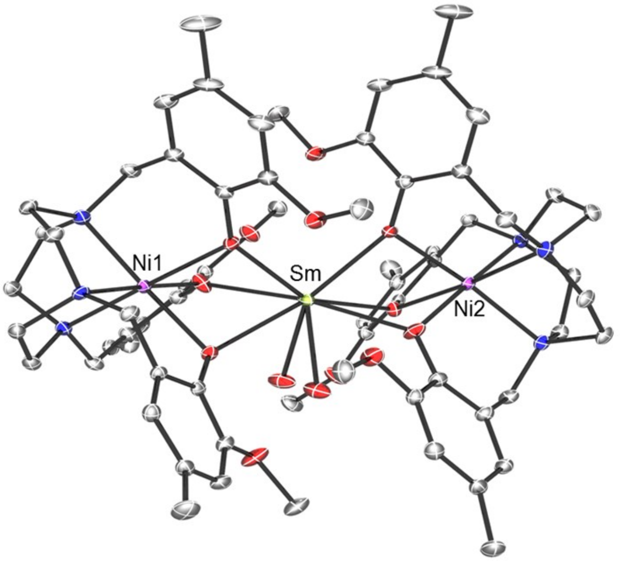

j)

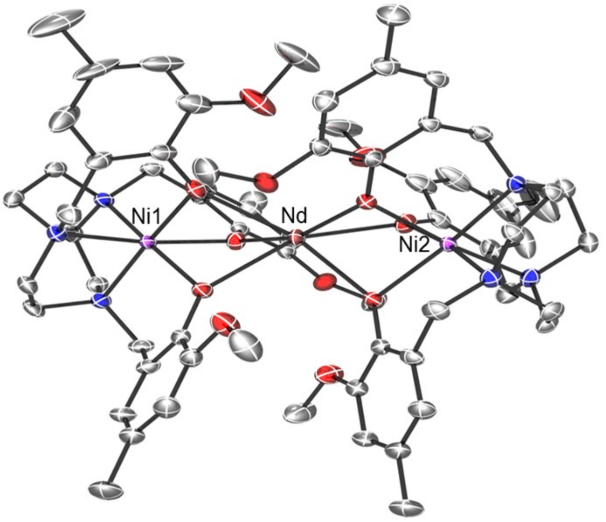

**Figure S1.** continued

k)

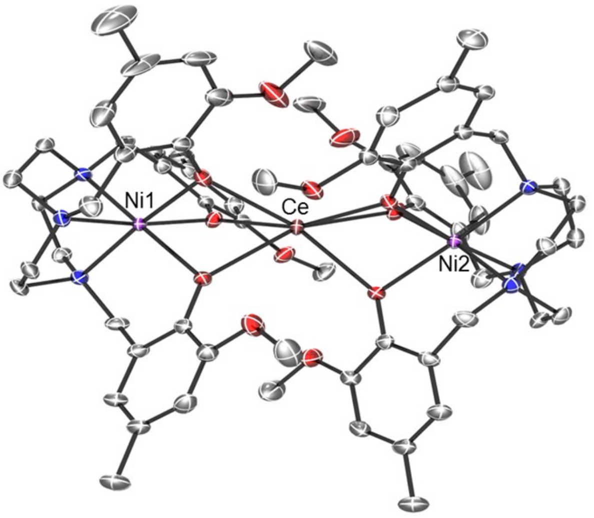

l)

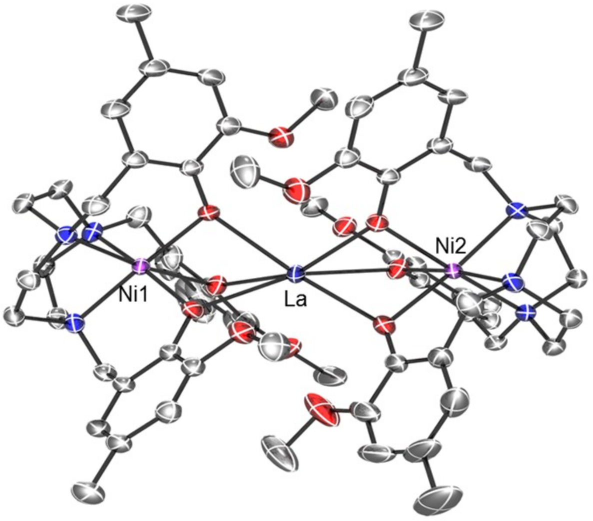

**Figure S1.** continued

m)

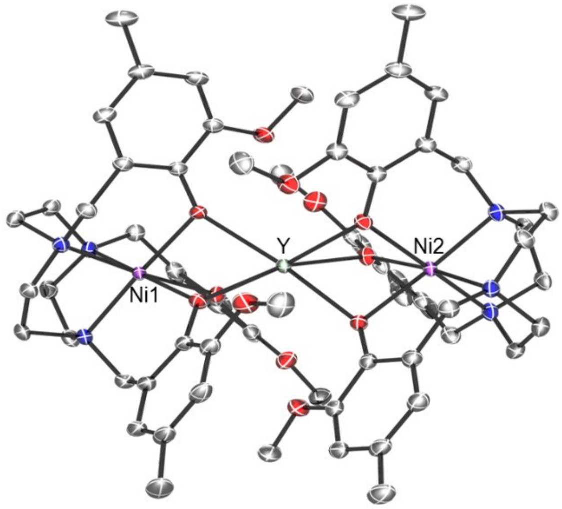

**Figure S1.** continued

# 2. Magnetism

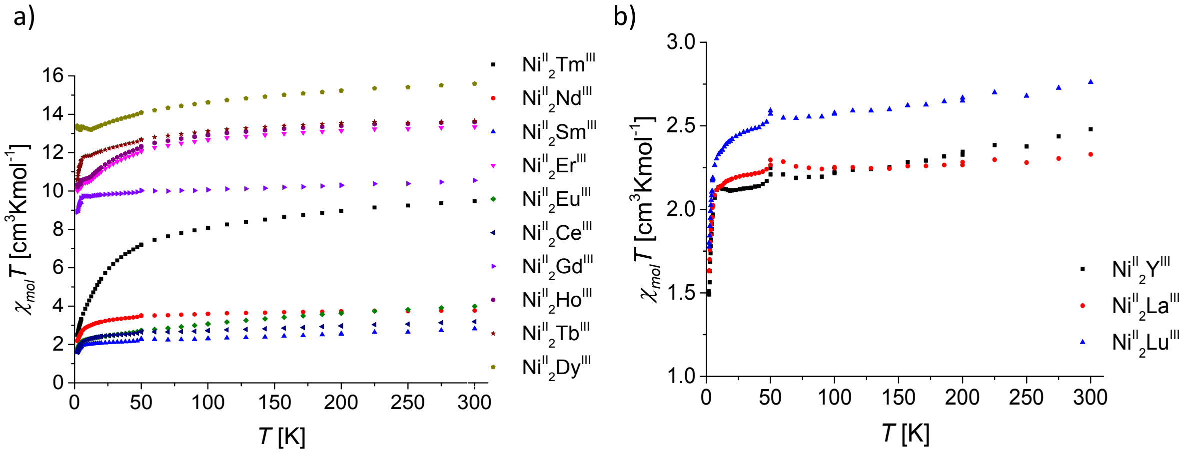

**Figure S2.** $\chi_{\mathrm{mol}}T$ vs. $T$ for the trinuclear Ni(II)$_2$Ln compounds with a) para- and b) diamagnetic lanthanide ions; data measured between 2.0 K and 300.0 K, with an applied field of 0.05 T; the mass of the samples was between 15 mg and 40 mg; the diamagnetic contribution was calculated using Pascal's constants; the anomaly at approx. 50K is due to condensed $O_2$ in the samples.

For the compounds Ni(II)$_2$Y(III), Ni(II)$_2$La(III) and Ni(II)$_2$Lu(III) with two unpaired electrons the $\chi_{\mathrm{mol}}$T values at 300 K should theoretically be 2.0 cm$^3$Kmol$^{-1}$ but are significantly higher with 2.48 cm$^3$Kmol$^{-1}$, 2.33 cm$^3$Kmol$^{-1}$ and 2.76 cm$^3$Kmol$^{-1}$. It is expected that the diamagnetic lanthanides can induce small geometric changes and therefore slightly different ligand fields at the Ni(II) centers, which lead to significantly different magnetic properties in the three compounds. A fit for the reduced magnetization can be obtained by fitting with the program JulX.[17]

The magnetization for Ni(II)$_2$Y(III) at 2.0 and 5.0 K versus the applied fields from 0.0 to 5.0 T is provided in Figure S3. The magnetizations are simulated by Brillouin functions. The best fit at both temperatures leads to g values of 2.0 for the two Ni(II) ions (S=1). The reduced magnetization (M vs. H/T) shows a splitting of the isofield lines, which indicates a zero field splitting. The best fit leads to $J_{\mathrm{Ni-Ni}}$ = -0.294 cm$^{-1}$, $g_{\mathrm{Ni}}$ = 2.09, $D_{\mathrm{Ni}}$ = 1.933 cm$^{-1}$ und $E/D$ = 0.154.

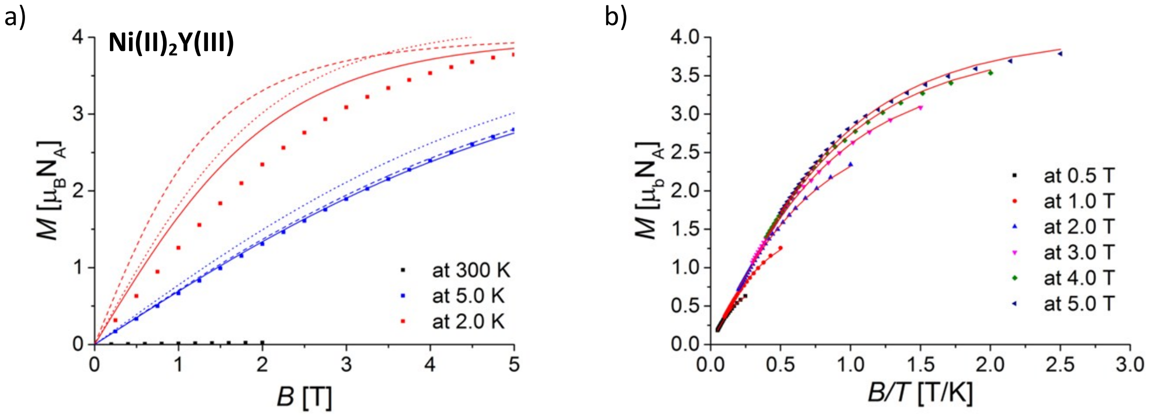

**Figure S3.** a) $M$ vs. applied field $B$ and b) reduced magnetization ($M$ vs. $B/T$) plots for Ni(II)$_2$Y(III). For a) the red and blue lines show the simulations for two Ni(II) ($g$ = 2.0, $S$ = 1.0; —), two Ni(II) ($g$ = 2.0, $S$ = 2.0; · · ·), two Ni(II) ($g$ = 2.0, $S$ = 2.0; - - -), two Ni(II) ($g$ = 1.977, $S$ = 1.0; —), two Ni(II) ($g$ = 2.094 $S$ = 1.0; · · ·) and ($g$ = 2.0, $S$ = 1.0; - - -); for b) $J_{\text{Ni-Ni}}$ = -0.294 cm$^{-1}$, $g_{\text{Ni}}$ = 2.094, $D_{\text{Ni}}$ = 1.933 cm$^{-1}$ and $E/D$ = 0.154 (—).

The magnetization for Ni(II)$_2$Lu(III) at 2.0 K can be simulated with a Brillouin function for two Ni(II) ions (S=1) with a g value of 2.00 (Figure S4). At 5.0 K the best fit is obtained for two Ni(II) ions (S=1) with g values of 2.06. The reduced magnetization also shows a splitting of the isofield lines. These are best fitted with $J_{\text{Ni-Ni}}$ = -0.129 cm$^{-1}$, $g_{\text{Ni}}$ = 2.18, $D_{\text{Ni}}$ = 2.838 cm$^{-1}$ and $E/D$ = 0.468.

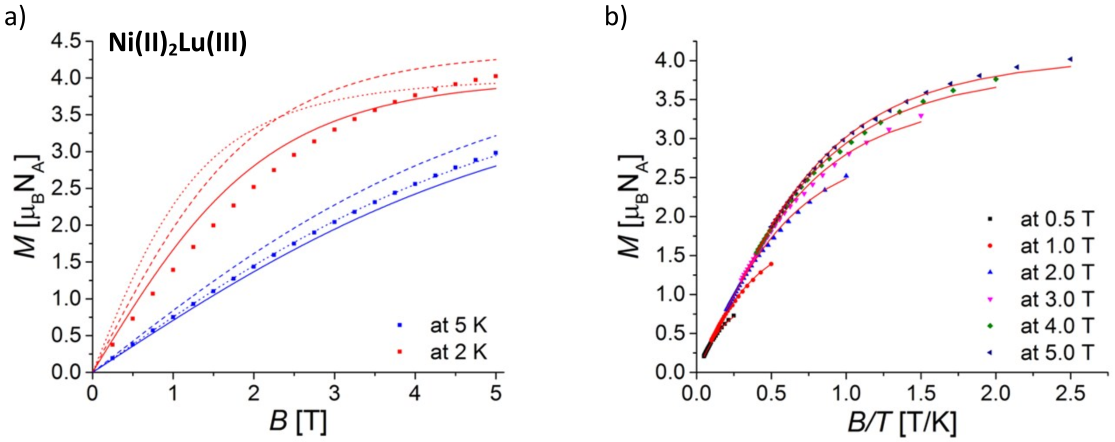

**Figure S4.** $M$ vs. applied field $B$ and b) reduced magnetization ($M$ vs. $B/T$) plots for Ni(II)$_2$Lu(III). For a) the red and blue lines show the fits for two Ni(II) ($g$ = 2.0, $S$ = 1.0; —), two Ni(II) ($g$ = 2.0, $S$ = 2.0; · · ·), two Ni(II) ($g$ = 2.182, $S$ = 1.0; - - -), two Ni(II) ($g$ = 2.0, $S$ = 1.0; —), two Ni(II) ($g$ = 2.063 $S$ = 1.0; · · ·) and ($g$ = 2.182, $S$ = 1.0; - - -); for b) $J_{\text{Ni-Ni}}$ = -0.129 cm$^{-1}$, $g_{\text{Ni}}$ = 2.182, $D_{\text{Ni}}$ = 2.838 cm$^{-1}$ und $E/D$ = 0.468 (—).

A comparison of Ni(II)$_2$Y(III) with Ni(II)$_2$Lu(III) confirms a small anisotropy for the Ni(II) ions and a weak coupling between the two centers. The g values lie in the range of literature known Ni(II) compounds.

With the help of PHI[18] it was possible to fit the magnetic data of Ni(II)$_2$Gd(III). The isotropic fit uses the susceptibility vs. temperature data together with the reduced magnetization data. The corresponding fits are presented in Figure S5. These result in $J_{\text{Ni-Ni}}$ = -0.377 cm$^{-1}$, $J_{\text{Gd-Ni}}$ = -0.009 cm$^{-1}$, $g_{\text{Ni}}$ = 2.102, $g_{\text{Gd}}$ = 1.974 and $\chi_{\mathrm{TIP}}$ = 0.003 cm$^3$Kmol$^{-1}$. This indicates a very weak interaction between the Gd(III) an Ni(II) ions.

Magnetic ac Squid measurements show no signals in the measurement range for the Ni(II)$_2$Ho(III), Ni(II)$_2$Dy(III) und Ni(II)$_2$Tb(III). Applied dc fields show no deceleration of the relaxation time.

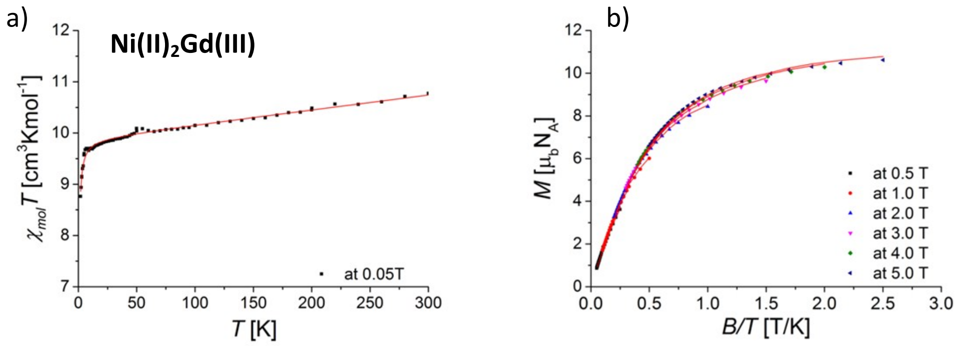

**Figure S5.** a) $\chi_{mol}T$ versus temperature (applied field of 0.05 T) and b) reduced magnetization (*M* vs. *H/T*) plots for Ni(II)$_2$Gd(III). The red lines (— ) follow the fit with the parameters $J_{\text{Ni-Ni}}$ = -0.377 cm$^{-1}$, $J_{\text{Gd-Ni}}$ = -0.009 cm$^{-1}$, $g_{\text{Ni}}$ = 2.102, $g_{\text{Gd}}$ = 1.974 and $\chi_{\mathrm{TIP}}$ = 0.003 cm$^3$Kmol$^{-1}$ for Ni(II)$_2$Gd(III).

# 3. Paramagnetic NMR Spectroscopy

1,2-Dichlorobenzene-$d_4$ was obtained from deutero GmbH (>99%) and dried before use by distillation from CaH$_2$. The temperature adjustment in the NMR spectrometers was calibrated for the used gas flow rate using a standard substance (ethylene glycol). Raw data were processed using a back-prediction macro which was adjusted for each individual sample. Due to the large shift range the phasing of the spectra is to some degree arbitrary. Consequently, especially for signals with large chemical shifts uncertainties of the shift values of up to 5 ppm are possible.

*Interpretation of chemical shifts*

In accordance with the literature, additive effects of the different paramagnetic centers were assumed. The chemical shift produced by the proximal and distal Ni atoms (Ni,p and Ni,d, respectively) as well as the lanthanide ion can each be separated into a Fermi contact ($\delta_{con}$) and a pseudo contact ($\delta_{pc}$) contribution. Consequently, the total chemical shift observed can be described by Eq. S1.

$$\delta_{obs} = \delta_{orb} + \delta_{con}^{Ni,p} + \delta_{pc}^{Ni,p} + \delta_{con}^{Ni,d} + \delta_{pc}^{Ni,d} + \delta_{con}^{Ln} + \delta_{pc}^{Ln} \qquad \text{(S1)}$$

In order to simplify this equation, several assumptions were made. Firstly, as the Ni atoms are in a relatively symmetrical environment, their corresponding pseudo contact contributions are considered to be very small. This argument is backed up by the good agreement of the shifts calculated by DFT for the $Ni^{II}_2Y^{III}$ compound (which do not include pseudo contact shifts from $Ni^{II}$) with the experimental values. Furthermore, CASSCF calculations for the $Ni^{II}_2Dy^{III}$ compound also determined small anisotropies in the g values of the $Ni^{II}$ ions. Secondly, it is assumed that spin density of the $Ni^{II}$ ions is only transferred to the directly attached ligand. Spin density from the distal $Ni^{II}$ ion would have to be delocalized across the lanthanide ion. This assumption was supported by spin density calculations of an isostructural $Ni^{II}Y^{III}Zn^{II}$ complex, which showed identical values for the spin density in the ligand bound to the $Ni^{II}$ ion. Finally, contact shift contributions of lanthanide ions are typically small, especially for nuclei located several bonds away from the $Ln^{III}$ ion. This observation is commonly attributed due to the concentration of the unpaired electrons in *f* orbitals, which exhibit only minor delocalization compared to *d* orbitals. Deviations from this behavior would only be expected for nuclei very close (in terms of bonds) to the lanthanide ion, in our case especially the $C^5$ atom. Hence, several terms in Eq. S1 are assumed to equal zero, resulting in Eq. S2.

$$\delta_{obs} = \delta_{orb} + \delta_{con}^{Ni,p} + \delta_{pc}^{Ln} \qquad \text{(S2)}$$

The first two terms in this equation describe the chemical shifts expected for the $Ni^{II}_2Y^{III}$ compound. They can be obtained with reasonable accuracy by DTF calculations, which show good agreement with the chemical shift values obtained for the $Ni^{II}_2Y^{III}$ compound. The last term represents the effect of the lanthanide ion and was used for obtaining χ values.

*Determination of χ tensors and $\Delta\chi_{ax}$ values*

Tensor components were obtained by fitting the following formula (S3) to the observed lanthanide pseudo contact shift values $\delta_{pc}$.

$$\delta_{pc} = \frac{1}{4\pi r^3}\left[(\chi_{zz} - \overline{\chi})\bullet\frac{2z^2 - x^2 - y^2}{2r^2} + (\chi_{xx} - \chi_{yy})\bullet\frac{x^2 - y^2}{2r^2} + \chi_{xy}\bullet\frac{2xy}{r^2} + \chi_{xz}\bullet\frac{2xz}{r^2} + \chi_{yz}\bullet\frac{2yz}{r^2}\right] \qquad \text{(S3)}$$

Therein, x,y and z are the coordinates of the investigated nucleus with respect to the lanthanide ion in an arbitrary reference frame, r represents the distance, i.e.

$$r = \sqrt{x^2 + y^2 + z^2} \qquad \text{(S4)}$$

$\chi_{ii}$ are the values of the susceptibility tensor in the arbitrary reference frame.

$$\chi = \begin{pmatrix} \chi_{xx} & \chi_{xy} & \chi_{xz} \\ \chi_{xy} & \chi_{yy} & \chi_{yz} \\ \chi_{xz} & \chi_{yz} & \chi_{zz} \end{pmatrix} \qquad \text{(S5)}$$

The trace of the tensor is independent of the chosen reference frame and defined as:

$$\overline{\chi} = \frac{1}{3}(\chi_{xx} + \chi_{yy} + \chi_{zz}) \qquad \text{(S6)}$$

The components of the χ tensor were fitted using a customized fitting function (based on the above equation) in the program Origin (version 9.1G). As the absolute value of χ cannot be determined by this method, only five of the six $\chi_{ii}$ components are independent. Hence, the $\chi_{yy}$ value was fixed for the fitting procedure.

At the final stage methyl groups were included in the fitting procedure. In these cases complications arise due to the different positions for the hydrogen nuclei produced by rotations about the corresponding single bonds. As only one signal is observed for these groups, this is interpreted as the arithmetic average of the positions of the three corresponding atoms:

$$\overline{\delta_{pc}} = \frac{1}{n}\bullet\sum_{i=1}^{n}\delta_{pc,i} \qquad \text{(S7)}$$

Rearrangement of S3 gives:

$$\delta_{pc} = \frac{1}{4\pi}\left[(\chi_{zz} - \overline{\chi}) \bullet f_1 + (\chi_{xx} - \chi_{yy}) \bullet f_2 + \chi_{xy} \bullet f_3 + \chi_{xz} \bullet f_4 + \chi_{yz} \bullet f_5\right] \qquad \text{(S8)}$$

With the coordinate-dependent factors:

$$f_1 = \frac{2z^2 - x^2 - y^2}{2r^5}\,;\, f_2 = \frac{x^2 - y^2}{2r^5}\,;\, f_3 = \frac{2xy}{r^5}\,;\, f_4 = \frac{2xz}{r^5}\,;\, f_5 = \frac{2yz}{r^5} \qquad \text{(S9)}$$

Substituting S8 in S7 gives:

$$\overline{\delta_{pc}} = \frac{1}{n} \bullet \sum_{i=1}^{n}\left\{\frac{1}{4\pi}\left[(\chi_{zz} - \overline{\chi}) \bullet f_{1,i} + (\chi_{xx} - \chi_{yy}) \bullet f_{2,i} + \chi_{xy} \bullet f_{3,i} + \chi_{xz} \bullet f_{4,i} + \chi_{yz} \bullet f_{5,i}\right]\right\} \qquad \text{(S10)}$$

This can be rearranged to:

$$\overline{\delta_{pc}} = \frac{1}{n} \bullet \frac{1}{4\pi} \bullet \left[\sum_{i=1}^{n}(\chi_{zz} - \overline{\chi}) \bullet f_{1,i} + \sum_{i=1}^{n}(\chi_{xx} - \chi_{yy}) \bullet f_{2,i} + \sum_{i=1}^{n}\chi_{xy} \bullet f_{3,i} + \sum_{i=1}^{n}\chi_{xz} \bullet f_{4,i} + \sum_{i=1}^{n}\chi_{yz} \bullet f_{5,i}\right] \qquad \text{(S11)}$$

Factoring out the tensor values gives:

$$\overline{\delta_{pc}} = \frac{1}{n} \bullet \frac{1}{4\pi} \bullet \left[(\chi_{zz} - \overline{\chi}) \bullet F_1 + (\chi_{xx} - \chi_{yy}) \bullet F_i + \chi_{xy} \bullet F_3 + \chi_{xz} \bullet F_4 + \chi_{yz} \bullet F_5\right] \qquad \text{(S12)}$$

With the coordinate-dependent factor sums:

$$F_1 = \sum_{i=1}^{n}\frac{2{z_i}^2 - {x_i}^2 - {y_i}^2}{2{r_i}^5}\,;\, F_2 = \sum_{i=1}^{n}\frac{{x_i}^2 - {y_i}^2}{2{r_i}^5}\,;\, F_3 = \sum_{1=1}^{n}\frac{2x_i y_i}{{r_i}^5}\,;\, F_4 = \sum_{1=1}^{n}\frac{2x_i z_i}{{r_i}^5}\,;\, F_3 = \sum_{1=1}^{n}\frac{2y_i z_i}{{r_i}^5} \qquad \text{(S13)}$$

Correspondingly, the values for $F_1$ to $F_5$ were calculated for each methyl group and used for the fitting procedure. In all cases a very small improvement of the fit quality (as judged by the adjusted $R^2$ value) was observed. In principle all observed signals should be considered as arithmetic averages arising from the equivalent positions in the six ligand arms in the compounds. Consequently, an attempt was made to fit all observed pseudo contact shifts to the F values of the corresponding signal. However, no useful values were obtained in this way. This is apparently due to the fact, that the best fit produces very large pseudo contact shift values (>10000 ppm) with different signs for atoms contributing to the same signal, which are mostly averaged out but produce a very good agreement with the observed values.

The obtained χ tensors were diagonalized using the program Octave (version 3.8.1).[19] The tensor is then written as:

$$\tilde{\chi} = \begin{pmatrix} \tilde{\chi}_{xx} & 0 & 0 \\ 0 & \tilde{\chi}_{yy} & 0 \\ 0 & 0 & \tilde{\chi}_{zz} \end{pmatrix} \tag{S14}$$

$\Delta\chi_{ax}$ and $\Delta\chi_{rh}$ values were obtained from:

$$\Delta\chi_{ax} = \tilde{\chi}_{zz} - \frac{\tilde{\chi}_{xx} + \tilde{\chi}_{yy}}{2}\ ;\ \Delta\chi_{rh} = \tilde{\chi}_{xx} - \tilde{\chi}_{yy} \tag{S15}$$

It was assumed that the uncertainties of $\chi_{XX}$ and $\chi_{ZZ}$ as obtained from the fitting procedure are good estimates for the corresponding values after tensor diagonalization. With the fixed $\chi_{YY}$ value the uncertainty of the $\Delta\chi_{ax}$ value was then estimated as:

$$\begin{gathered} u(\Delta\chi_{ax}) = \left|\frac{\partial\Delta\chi_{ax}}{\partial\tilde{\chi}_{ZZ}}\right| \bullet u(\tilde{\chi}_{ZZ}) + \left|\frac{\partial\Delta\chi_{ax}}{\partial\tilde{\chi}_{XX}}\right| \bullet u(\tilde{\chi}_{XX}) \\ u(\Delta\chi_{ax}) = u(\tilde{\chi}_{ZZ}) + \frac{1}{2} \bullet u(\tilde{\chi}_{XX}) \end{gathered} \tag{S16}$$

The linewidths of the NMR signals discussed here depend on both the $\mathrm{Ni^{II}}$ and the $\mathrm{Ln^{III}}$ ion. In addition, the relaxation effects of the paramagnetic d- and f-block ions influence each other (*i.e.* the fast relaxing f-ion enhances the relaxation of the $\mathrm{Ni^{II}}$ ion). Therefore, the replacement of the diamagnetic $\mathrm{Y^{III}}$ ion by a paramagnetic $\mathrm{Ln^{III}}$ ion leads to an increase in NMR line widths for nuclei close to $\mathrm{Ln^{III}}$ but to a decrease for those nuclei which are close to $\mathrm{Ni^{II}}$ (and far from $\mathrm{Ln^{III}}$). This is exactly what is observed, see Table S2.

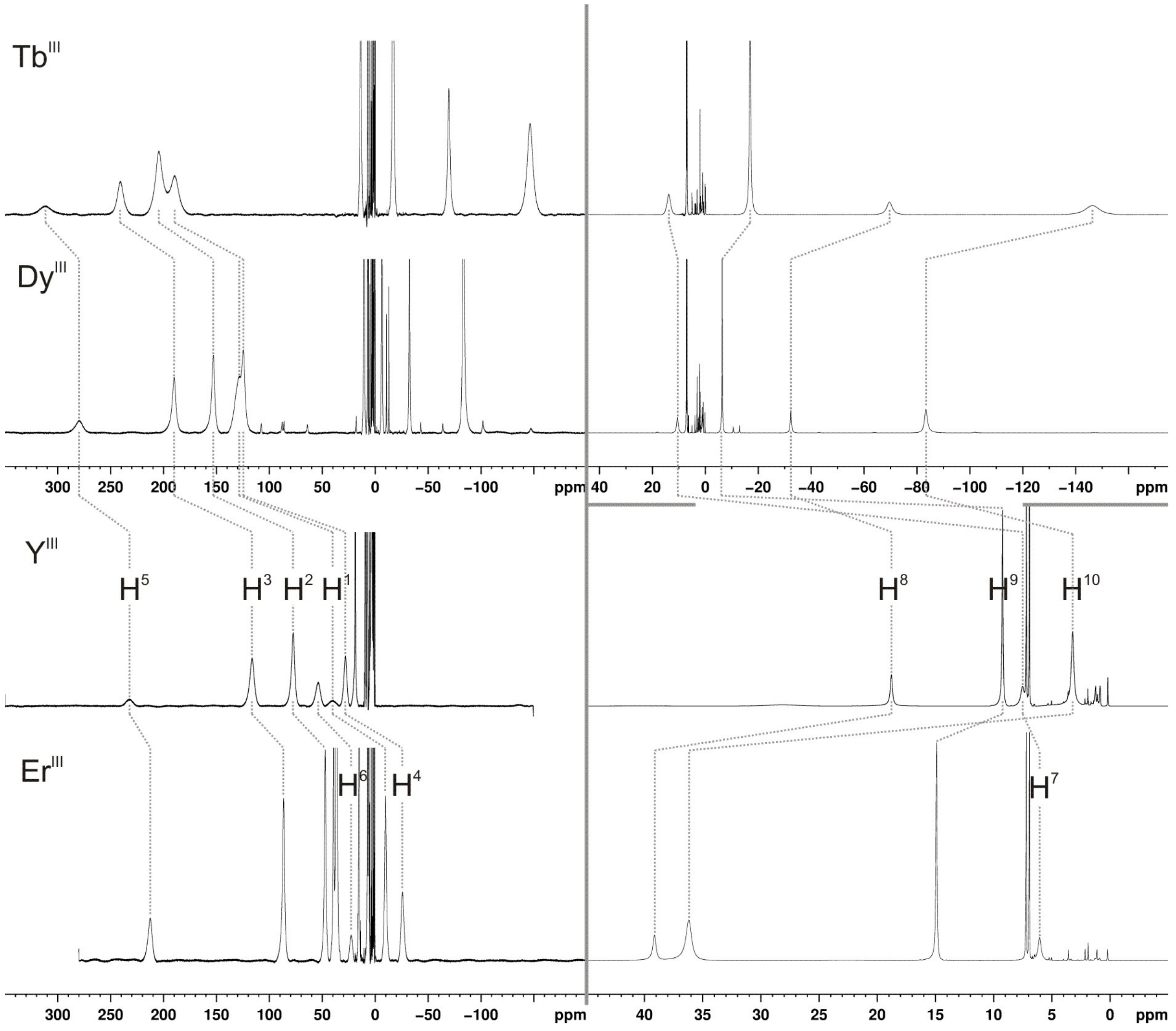

**Figure S6.** Stacked $^1$H NMR spectra (340 K, 600 MHz, $o$-$C_6D_4Cl_2$) of the $Ni^{II}_2Tb^{III}$, $Ni^{II}_2Dy^{III}$, $Ni^{II}_2Y^{III}$ and $Ni^{II}_2Er^{III}$ compounds (top to bottom) with labeling of individual signals. On the left side the entire signal range is displayed: Please note, that the enlargements on the right side have different axes for Tb$^{III}$/Dy$^{III}$ and Y$^{III}$/Er$^{III}$. A minor impurity is visible in the Dy$^{III}$ compound which possibly formed during the VT-experiments.

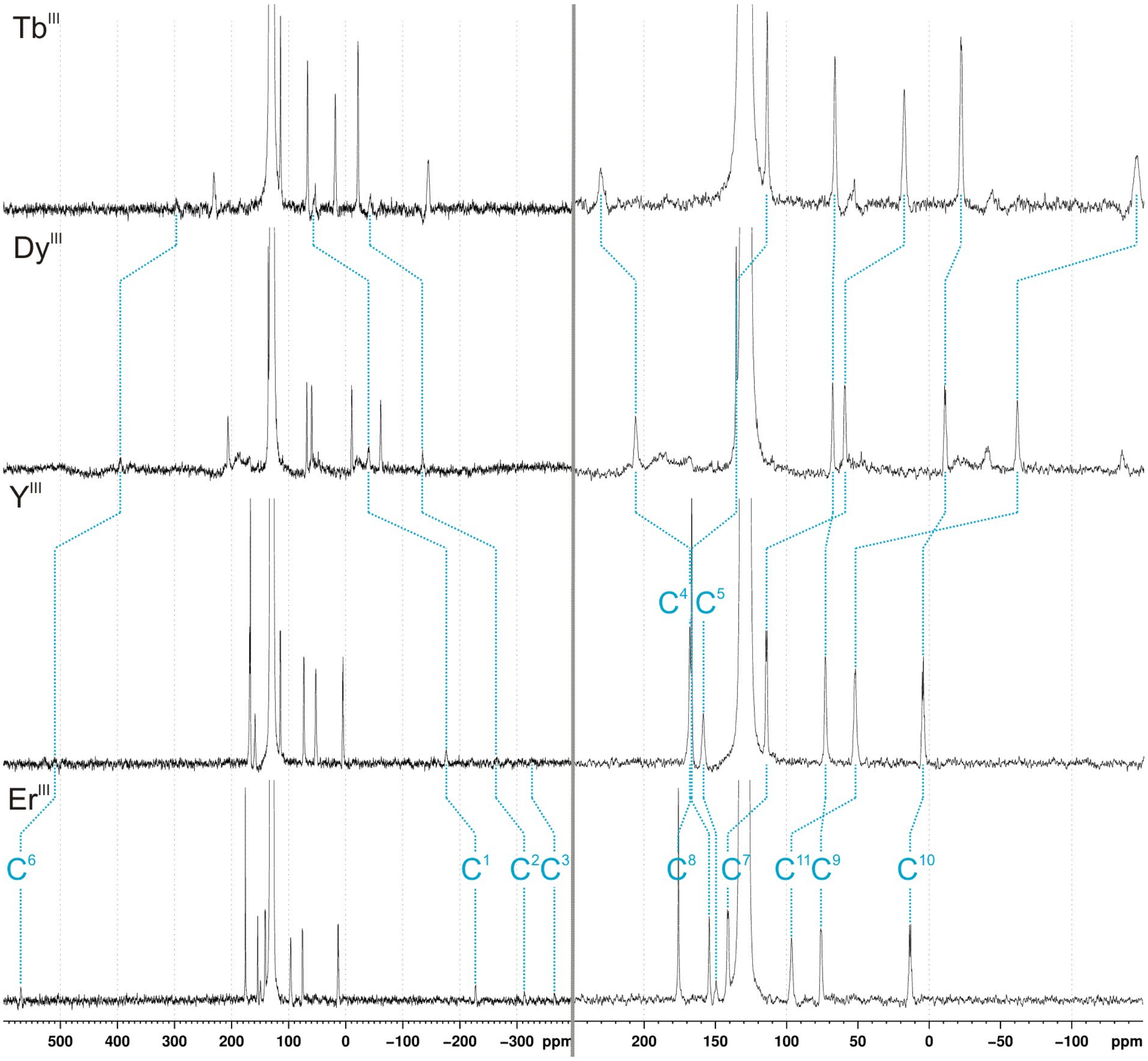

**Figure S7.** Stacked $^{13}$C NMR spectra (340 K, 150 MHz, *o*-$C_6D_4Cl_2$) of the $Ni^{II}_2Tb^{III}$, $Ni^{II}_2Dy^{III}$, $Ni^{II}_2Y^{III}$ and $Ni^{II}_2Er^{III}$ compounds (top to bottom) with labeling of individual signals. On the left side the entire signal range is displayed, the right side is an enlargement of the central part.

**Table S2.** Observed $^{1}$H NMR shifts (340K, 600 MHz, *o*-$C_6D_4Cl_2$) for the $Ni^{II}_2Y^{III}$, $Ni^{II}_2Er^{III}$, $Ni^{II}_2Dy^{III}$ and $Ni^{II}_2Tb^{III}$ compounds. Line widths were obtained from deconvolution.

| $Ln^{III}$ | $Y^{III}$ | | $Er^{III}$ | | $Dy^{III}$ | | $Tb^{III}$ | |
|---|---|---|---|---|---|---|---|---|
| Group | $\delta_{obs}$ (ppm) | $\Delta\nu_{1/2}$ (Hz) | $\delta_{obs}$ (ppm) | $\Delta\nu_{1/2}$ (Hz) | $\delta_{obs}$ (ppm) | $\Delta\nu_{1/2}$ (Hz) | $\delta_{obs}$ (ppm) | $\Delta\nu_{1/2}$ (Hz) |
| $H^1$ | 40.4 | 3825 | -9.8 | 1020 | 124.7 | 2243 | 189.5 | 5000 |
| $H^2$ | 77.5 | 1811 | 47.2 | 903.1 | 153.1 | 1801 | 204.7 | 4808 |
| $H^3$ | 116.2 | 2465 | 86.5 | 1238 | 190.1 | 2241 | 241 | 3416 |
| $H^4$ | 28 | 1614 | -25.8 | 1579 | 128.8 | 4393 | not observed | |
| $H^5$ | 232.2 | 3468 | 212.6 | 2057 | 279.7 | 3927 | 312.2 | 4300 |
| $H^6$ | 53.9 | 2528 | 22.7 | 1459 | not observed | | not observed | |
| $H^7$ | 7.5 | 214.0 | 6.1 | 182.1 | 10.6 | 416.5 | 13.8 | 791.8 |
| $H^8$ | 18.8 | 130.7 | 39.1 | 200.0 | -32.3 | 302.6 | -69.6 | 1366 |
| $H^9$ | 9.2 | 54.8 | 14.9 | 62.6 | -6.3 | 113.9 | -16.9 | 334.5 |
| $H^{10}$ | 3.2 | 157.9 | 36.2 | 335.7 | -83.3 | 740.7 | -151 | 3251 |

**Table S3.** Observed $^{13}$C NMR shifts (340 K, 150 MHz, *o*-$C_6D_4Cl_2$) for the $Ni^{II}_2Y^{III}$, $Ni^{II}_2Er^{III}$, $Ni^{II}_2Dy^{III}$ and $Ni^{II}_2Tb^{III}$ compounds. Values marked with an asterisk correspond to very broad and weak signals.

| | $\delta_{obs}$ (ppm) for $Ln^{III}$ = | | | |
|---|---|---|---|---|
| Group | $Y^{III}$ | $Er^{III}$ | $Dy^{III}$ | $Tb^{III}$ |
| $C^1$ | -175.5 | -227.2 | -39.8 | 56 |
| $C^2$ | -264.4* | -313* | -134.3* | -42.6 |
| $C^3$ | -322.5* | -365.8* | not observed | not observed |
| $C^4$ | 168.5 | 154.4 | 207 | 230.7 |
| $C^5$ | 159.1 | 149.6 | not observed | not observed |
| $C^6$ | 509.0* | 569.5 | 396* | 297* |
| $C^7$ | 114.8 | 141.3 | 60.1 | 18 |
| $C^8$ | 167.2 | 176 | 136.4 | 114.2 |
| $C^9$ | 73.5 | 76.3 | 68.7 | 66.7 |
| $C^{10}$ | 5.1 | 13.5 | -10.1 | -21.9 |
| $C^{11}$ | 52.7 | 96.6 | -60.9 | -144.8 |

**Table S4.** Calculated (B3LYP, 6-311G*/SDD) $\delta_{orb}$, $\delta_{con}^{Ni}$ and $\delta_{calc}$ values for the $Ni^{II}_2Y^{III}$ compound. Values are referenced against tetramethylsilane (TMS).

| | δ ($^1$H) [ppm] | | | | δ ($^{13}$C) [ppm] | | |
|---|---|---|---|---|---|---|---|
| Group | $\delta_{orb}$ | $\delta_{con}^{Ni}$ | $\delta_{calc}$ | Group | $\delta_{orb}$ | $\delta_{con}^{Ni}$ | $\delta_{calc}$ |
| $H^1$ | 2.4 | 24.9 | 27.3 | $C^1$ | 62.2 | -200.4 | -138.2 |
| $H^2$ | 2.8 | 74.6 | 77.5 | $C^2$ | 54.7 | -301.4 | -246.7 |
| $H^3$ | 2.1 | 124.4 | 126.5 | $C^3$ | 67.7 | -405.0 | -337.4 |
| $H^4$ | 2.4 | 15.2 | 17.6 | $C^4$ | 129.9 | 47.0 | 176.9 |
| $H^5$ | 3.3 | 215.6 | 218.9 | $C^5$ | 160.2 | 5.5 | 165.7 |
| $H^6$ | 4.8 | 48.4 | 53.2 | $C^6$ | 160.3 | 356.6 | 516.9 |
| $H^7$ | 6.7 | 2.8 | 9.4 | $C^7$ | 117.1 | -6.9 | 110.2 |
| $H^8$ | 6.5 | 13.8 | 20.3 | $C^8$ | 134.1 | 48.4 | 182.5 |
| $H^9$ | 2.3 | 9.7 | 12.0 | $C^9$ | 128.4 | -56.7 | 71.7 |
| $H^{10}$ | 3.3 | 0.0 | 3.3 | $C^{10}$ | 23.7 | -22.1 | 1.5 |
| | | | | $C^{11}$ | 56.1 | -2.8 | 53.4 |

**Table S5.** Observed and calculated (B3LYP, 6-311G*/SDD) $^1$H and $^{13}$C shifts for the $Ni^{II}_2Y^{III}$ compound. Values are referenced against TMS.

| | δ ($^1$H) [ppm] | | | δ ($^{13}$C) [ppm] | |
|---|---|---|---|---|---|
| Group | $\delta_{calc}$ | $\delta_{obs}$ | Group | $\delta_{calc}$ | $\delta_{obs}$ |
| $H^1$ | 27.3 | 40.5 | $C^1$ | -138.2 | -175.0 |
| $H^2$ | 77.5 | 77.5 | $C^2$ | -246.7 | -264.7 |
| $H^3$ | 126.5 | 116.2 | $C^3$ | -337.4 | -322.5 |
| $H^4$ | 17.6 | 28.1 | $C^4$ | 176.9 | 168.7 |
| $H^5$ | 218.9 | 232.4 | $C^5$ | 165.7 | 159.1 |
| $H^6$ | 53.2 | 53.9 | $C^6$ | 516.9 | 509.0 |
| $H^7$ | 9.4 | 7.5 | $C^7$ | 110.2 | 115.0 |
| $H^8$ | 20.3 | 18.8 | $C^8$ | 182.5 | 167.3 |
| $H^9$ | 12.0 | 9.2 | $C^9$ | 71.7 | 73.8 |
| $H^{10}$ | 3.3 | 3.2 | $C^{10}$ | 1.5 | 5.4 |
| | | | $C^{11}$ | 53.4 | 52.9 |

**Table S6.** Observed $\delta_{pc}^{Ln}$ values for $Ni^{II}_2Er^{III}$, $Ni^{II}_2Dy^{III}$ and $Ni^{II}_2Tb^{III}$ compounds. Values are referenced against TMS. The value for $C_5$ of the $Ni^{II}_2Er^{III}$ compound (marked with an asterisk) probably contains a contribution of about -20 ppm.

| | $\delta_{pc}^{Ln}$ for $Ln^{III}$ = | | |
|---|---|---|---|
| Group | $Er^{III}$ | $Dy^{III}$ | $Tb^{III}$ |
| $H^1$ | -50.2 | 84.3 | 149.1 |
| $H^2$ | -30.3 | 75.6 | 127.2 |
| $H^3$ | -29.7 | 73.9 | 124.8 |
| $H^4$ | -53.8 | 100.8 | signal not observed |
| $H^5$ | -19.6 | 47.5 | 80 |
| $H^6$ | -31.2 | signal not observed | signal not observed |
| $H^7$ | -1.4 | 3.1 | 6.3 |
| $H^8$ | 20.3 | -51.1 | -88.4 |
| $H^9$ | 5.7 | -15.5 | -26.1 |
| $H^{10}$ | 33.0 | -86.5 | -154.2 |
| $C^1$ | -51.7 | 135.7 | 231.5 |
| $C^2$ | -48.6 | 130.1 | 221.8 |
| $C^3$ | -43.3 | signal not observed | signal not observed |
| $C^4$ | -14.1 | 30.1 | 62.2 |
| $C^5$ | -9.5* | signal not observed | signal not observed |
| $C^6$ | 60.5 | -113.0 | -212.0 |
| $C^7$ | 26.5 | -54.7 | -96.8 |
| $C^8$ | 8.8 | -30.8 | -53 |
| $C^9$ | 2.8 | -4.8 | -6.8 |
| $C^{10}$ | 8.4 | -15.2 | -27 |
| $C^{11}$ | 43.9 | -113.6 | -197.5 |

**Table S7.** Observed and calculated $\delta_{pc}^{Ln}$ values for the $Ni^{II}_2Er^{III}$ compound for different models. The calculated values correspond to the ones obtained from the refined tensor including correction for methyl group rotation. The "DFT-optimized" structure was obtained using the B3LYP functional and the 6-311G* basis set (with SDD for the $Ni^{II}$ and $Y^{III}$ ions). Adjusted $R^2$ values for the different fittings can be found in the last row.

| | $\delta_{pc}^{Ln}$ [ppm] | | | | |
|---|---|---|---|---|---|
| Group | measured | $Ni^{II}_2Er^{III}$ X-ray | $Ni^{II}_2Dy^{III}$ X-ray | $D_3$-symmetrized | DFT-optimized |
| $H^1$ | -50.2 | -40.5 | -40.2 | -40.9 | -40.1 |
| $H^2$ | -30.3 | -32.4 | -32.4 | -32.1 | -32.0 |
| $H^3$ | -29.7 | -32.4 | -32.4 | -32.7 | -31.7 |
| $H^4$ | -53.8 | -44.4 | -45.2 | -44.7 | -46.6 |
| $H^5$ | -19.6 | -20.7 | -21.7 | -21.4 | -21.1 |
| $H^6$ | -31.2 | -28.3 | -31.0 | -28.7 | -36.6 |
| $H^7$ | -1.4 | 1.4 | -1.2 | 1.1 | -2.2 |
| $H^8$ | 20.3 | 23.3 | 22.4 | 23.5 | 20.8 |
| $H^9$ | 5.7 | 7.9 | 6.3 | 8.2 | 5.8 |
| $H^{10}$ | 33.0 | 33.1 | 35.1 | 35.1 | 34.7 |
| $C^1$ | -51.7 | -54.9 | -54.6 | -55.1 | -56.3 |
| $C^2$ | -48.6 | -52.1 | -51.6 | -52.5 | -53.3 |
| $C^3$ | -43.3 | -43.1 | -44.2 | -44.9 | -47.4 |
| $C^4$ | -14.1 | -12.1 | -15.8 | -15.0 | -18.1 |
| $C^5$ | -9.5 | 13.9 | 6.7 | 5.4 | 2.4 |
| $C^6$ | 60.5 | 58.9 | 56.3 | 57.5 | 51.8 |
| $C^7$ | 26.5 | 27.8 | 25.6 | 27.7 | 23.9 |
| $C^8$ | 8.8 | 14.4 | 11.6 | 14.3 | 10.5 |
| $C^9$ | 2.8 | 5.6 | 2.2 | 5.0 | 0.9 |
| $C^{10}$ | 8.4 | 9.0 | 7.2 | 9.2 | 6.7 |
| $C^{11}$ | 43.9 | 42.8 | 45.6 | 45.3 | 45.1 |
| adj. $R^2$ | | 0.9725 | 0.9769 | 0.9830 | 0.9862 |

**Table S8.** Observed and calculated $\delta_{pc}^{Ln}$ values for the $Ni^{II}_2Dy^{III}$ compound for different models. The calculated values correspond to the ones obtained from the refined tensor including correction for methyl group rotation. The "DFT-optimized" structure was obtained using the B3LYP functional and the 6-311G* basis set (with SDD for the $Ni^{II}$ and $Y^{III}$ ions). Adjusted R² values for the different fittings can be found in the last row.

| | $\delta_{pc}^{Ln}$ [ppm] | | | | |
|---|---|---|---|---|---|
| Group | measured | $Ni^{II}_2Er^{III}$ X-ray | $Ni^{II}_2Dy^{III}$ X-ray | $D_3$-symmetrized | DFT-optimized |
| $H^1$ | 84.3 | 92.2 | 92.2 | 92.9 | 93.2 |
| $H^2$ | 75.6 | 73.7 | 74.3 | 72.9 | 74.4 |
| $H^3$ | 73.9 | 73.8 | 74.2 | 74.4 | 73.8 |
| $H^4$ | 100.8 | 101.2 | 103.6 | 101.6 | 108.3 |
| $H^5$ | 47.5 | 47.3 | 49.7 | 48.7 | 49.2 |
| $H^6$ | - | 64.6 | 71.1 | 65.3 | 85.1 |
| $H^7$ | 3.1 | -3.1 | 2.7 | -2.6 | 5.1 |
| $H^8$ | -51.1 | -53.0 | -51.4 | -53.4 | -48.4 |
| $H^9$ | -15.5 | -18.0 | -14.5 | -18.6 | -13.4 |
| $H^{10}$ | -86.5 | -75.4 | -80.5 | -79.9 | -80.6 |
| $C^1$ | 135.7 | 124.9 | 125.0 | 125.4 | 131.0 |
| $C^2$ | 130.1 | 118.8 | 118.2 | 119.3 | 124.0 |
| $C^3$ | - | 98.3 | 101.4 | 102.0 | 110.2 |
| $C^4$ | 30.1 | 27.6 | 36.3 | 34.1 | 42.1 |
| $C^5$ | - | -31.7 | -15.2 | -12.2 | -5.6 |
| $C^6$ | -113.0 | -134.3 | -129.1 | -130.7 | -120.5 |
| $C^7$ | -54.7 | -63.3 | -58.6 | -62.9 | -55.5 |
| $C^8$ | -30.8 | -32.8 | -26.5 | -32.4 | -24.3 |
| $C^9$ | -4.8 | -12.8 | -4.9 | -11.3 | -2.1 |
| $C^{10}$ | -15.2 | -20.4 | -16.4 | -20.9 | -15.5 |
| $C^{11}$ | -113.6 | -97.7 | -104.5 | -103.0 | -104.8 |
| adj. R² | | 0.9796 | 0.9854 | 0.9943 | 0.9902 |

**Table S9.** Observed and calculated $\delta_{pc}^{Ln}$ values for the $Ni^{II}_2Tb^{III}$ compound for different models. The calculated values correspond to the ones obtained from the refined tensor including correction for methyl group rotation. The “DFT-optimized” structure was obtained using the B3LYP functional and the 6-311G* basis set (with SDD for the $Ni^{II}$ and $Y^{III}$ ions). Adjusted $R^2$ values for the different fittings can be found in the last row.

| | $\delta_{pc}^{Ln}$ [ppm] | | | | |
|---|---|---|---|---|---|
| Group | measured | $Ni^{II}_2Er^{III}$ X-ray | $Ni^{II}_2Dy^{III}$ X-ray | $D_3$-symmetrized | DFT-optimized |
| $H^1$ | 149.1 | 161.7 | 162.0 | 164.5 | 162.9 |
| $H^2$ | 127.2 | 129.3 | 130.5 | 131.3 | 127.8 |
| $H^3$ | 124.8 | 129.4 | 130.4 | 130.2 | 130.3 |
| $H^4$ | - | 177.4 | 182.1 | 191.1 | 178.1 |
| $H^5$ | 80 | 82.9 | 87.4 | 86.7 | 85.3 |
| $H^6$ | - | 113.2 | 124.9 | 150.2 | 114.4 |
| $H^7$ | 6.3 | -5.5 | 4.8 | 9.0 | -4.5 |
| $H^8$ | -88.4 | -92.9 | -90.4 | -85.4 | -93.5 |
| $H^9$ | -26.1 | -31.6 | -25.5 | -23.7 | -32.6 |
| $H^{10}$ | -154.2 | -132.2 | -141.4 | -142.2 | -140.0 |
| $C^1$ | 231.5 | 219.1 | 219.7 | 231.2 | 219.7 |
| $C^2$ | 221.8 | 208.2 | 207.8 | 218.8 | 209.1 |
| $C^3$ | - | 172.4 | 178.2 | 194.5 | 178.8 |
| $C^4$ | 62.2 | 48.5 | 63.8 | 74.3 | 59.8 |
| $C^5$ | - | -55.5 | -26.8 | -9.9 | -21.5 |
| $C^6$ | -212.0 | -235.4 | -226.9 | -212.7 | -229.0 |
| $C^7$ | -96.8 | -111.0 | -103.1 | -97.9 | -110.2 |
| $C^8$ | -53 | -57.5 | -46.6 | -42.9 | -56.8 |
| $C^9$ | -6.8 | -22.4 | -8.6 | -3.6 | -19.8 |
| $C^{10}$ | -27 | -35.8 | -28.8 | -27.3 | -36.7 |
| $C^{11}$ | -197.5 | -171.3 | -183.8 | -184.9 | -180.5 |
| adj. $R^2$ | | 0,9825 | 0,9889 | 0,9968 | 0,9930 |

**Table S10.** $\Delta\chi_{ax}$ and $\Delta\chi_{rh}$ values for the $Ni^{II}_2Er^{III}$, $Ni^{II}_2Dy^{III}$ and $Ni^{II}_2Tb^{III}$ compounds obtained from the different models. Values correspond to the ones obtained from the refined tensor including correction for methyl group rotation.

| | $Ni^{II}_2Er^{III}$ X-ray | $Ni^{II}_2Dy^{III}$ X-ray | *$D_3$*-symmetrized | DFT-optimized |
|---|---|---|---|---|
| $Ni^{II}_2Er^{III}$ | | | | |
| $\Delta\chi_{ax}$ [$10^{-31}$ $m^3$] | -1.971±0.036 | -2.024±0.048 | -2.158±0.044 | -2.008±0.036 |
| $\Delta\chi_{rh}$ [$10^{-31}$ $m^3$] | -0.032±0.024 | -0.024±0.032 | 0±0.029 | 0±0.024 |
| $Ni^{II}_2Dy^{III}$ | | | | |
| $\Delta\chi_{ax}$ [$10^{-31}$ $m^3$] | 4.489±0.076 | 4.637±0.094 | 5.017±0.064 | 4.566±0.076 |
| $\Delta\chi_{rh}$ [$10^{-31}$ $m^3$] | 0.212±0.051 | 0.179±0.065 | 0±0.044 | -0.002±0.051 |
| $Ni^{II}_2Tb^{III}$ | | | | |
| $\Delta\chi_{ax}$ [$10^{-31}$ $m^3$] | 7.872±0.179 | 8.151±0.146 | 8.853±0.086 | 8.002±0.114 |
| $\Delta\chi_{rh}$ [$10^{-31}$ $m^3$] | 0.400±0.163 | 0.331±0.098 | 0±0.057 | -0.003±0.074 |

# 4. Ligand Synthesis

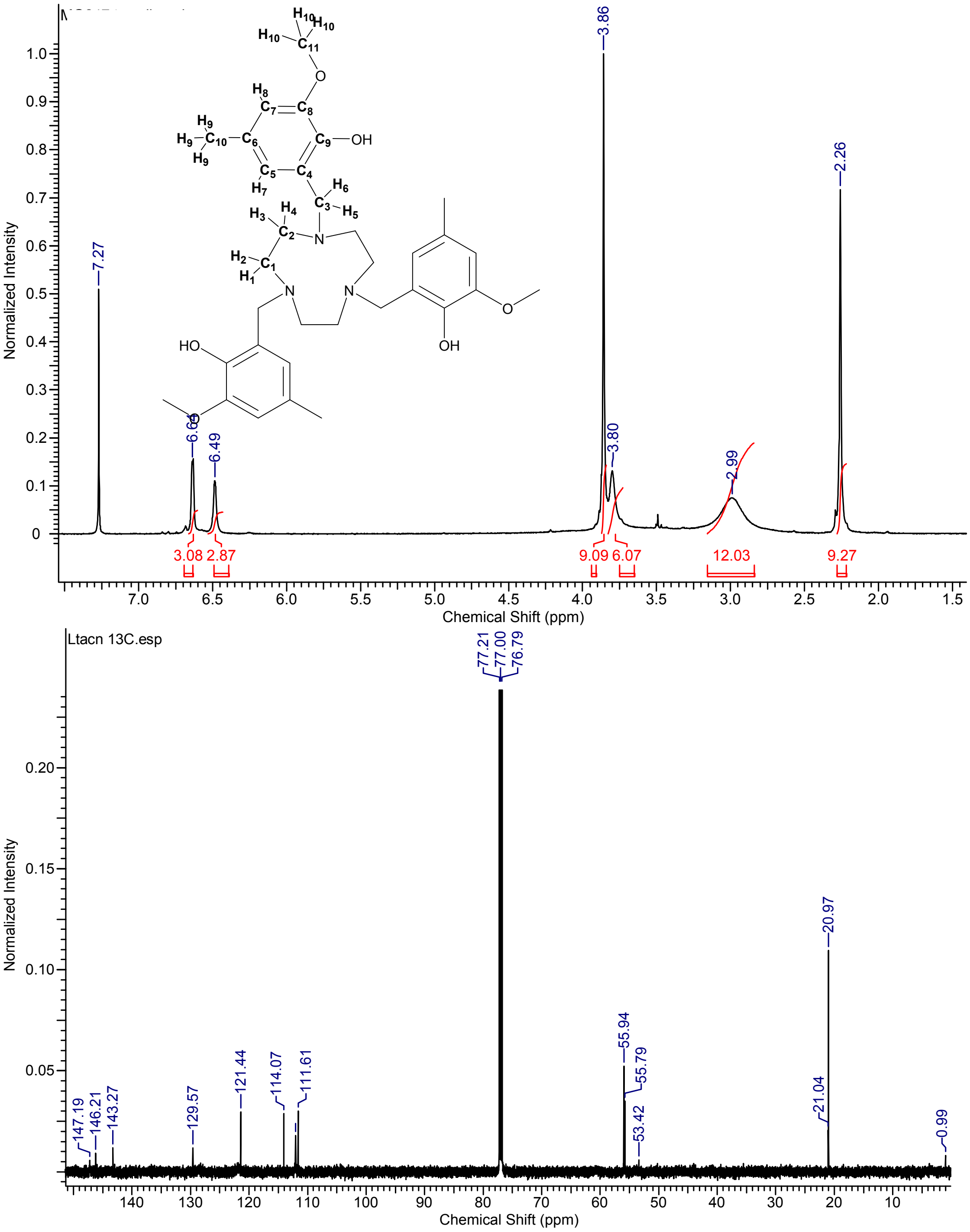

**Figure S8.** $^1$H- and $^{13}$C-NMR spectra of $H_3L$

# 5. References

1. *SAINT*, Bruker AXS GmbH, Karlsruhe, Germany: 1997-2013.
2. CrysAlisPro Agilent Technologies, UK Ltd., Oxford: 2011-2014.
3. Diffraction, R. O., *Rigaku Polska Sp.z.o.o., Wroclaw, Poland* **2015**.
4. Sheldrick, G. M. *SADABS*, Bruker AXS GmbH: Karlsruhe, Germany, 2004-2014.
5. Krause, L.; Herbst-Irmer, R.; Sheldrick, G. M.; Stalke, D., Comparison of silver and molybdenum microfocus X-ray sources for single-crystal structure determination. *J. Appl. Cryst.* **2015,** *48*, 3-10.
6. CrysAlisPro *SCALE3 ABSPACK CrysAlisPro*, Agilent Technologies UK Ltd.: Oxford, 2011-2014.
7. Blessing, R. H., An empirical correction for absorption anisotropy. *Acta Cryst.* **1995,** *A51*, 33-38.
8. Palatinus, L. SUPERFLIP; EPF Lausanne, Switzerland and Fyzikalni ustav AV CR, Prague, Czech Republic: 2007-2014.
9. Palatinus, L.; Chapuis, G., SUPERFLIP - a computer program for the solution of crystal structures by charge flipping in arbitrary dimensions. *J. Appl. Cryst.* **2007,** *40*, 786-790.
10. Sheldrick, G. M. SHELXL-20xx; University of Göttingen and Bruker AXS GmbH, Karlsruhe, Germany: 2012-2014.
11. Sheldrick, G. M., A short history of SHELX. *Acta Cryst.* **2008,** *A64*, 112-122.
12. Sheldrick, G. M., Crystal structure refinement with SHELXL. *Acta Cryst.* **2015,** *C71*, 3-8.
13. Sluis, P. v. d.; Spek, A. L., BYPASS: an effective method for the refinement of crystal structures containing disordered solvent regions. *Acta Cryst.* **1990,** *A46*, 194-201.
14. Spek, A. L., PLATON SQUEEZE: a tool for the calculation of the disordered solvent contribution of the calculated structure factors. *Acta Cryst.* **2015,** *C71*, 9-18.
15. Spek, A. L. PLATON, Utrecht University, The Netherlands: 2003.
16. Spek, A. L., Single-crystal structure validation with the program PLATON. *J. Appl. Cryst.* **2003,** *36*, 7-13.
17. Bill, E., 1.6 ed.; Mühlheim/Ruhr, 2008.
18. Chilton, N. F.; Anderson, R. P.; Turner, L. D.; Soncini, A.; Murray, K. S., *J. Comp. Chem.* **2013,** *34*, 1164-1175.
19. Eaton, J. W.; Bateman, D.; Hauberg, S., GNU Octave version 3.0.1 manual: a high-level interactive language for numerical computation. CreateSpace Independent Publishing Platform. **2009**.